

Neutron-star matter with the energy density functional theory

Nicolas Chamel

Institut d'Astronomie et d'Astrophysique
Université Libre de Bruxelles, Belgique



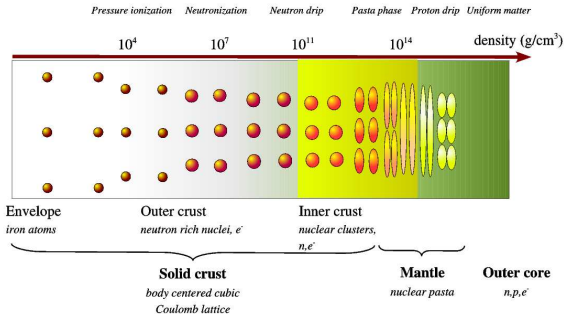
ULB



Gordon Conference, Colby-Sawyer College, 12-17 June 2011

Internal constitution of neutron stars

The interior of a neutron star contains **very different phases of matter**. A unified description of all regions of neutron stars is therefore very challenging.



Chamel&Haensel, *Living Reviews in Relativity* 11 (2008), 10
<http://relativity.livingreviews.org/Articles/lrr-2008-10/>

Nuclear energy density functional theory in a nut shell

The nuclear energy density functional theory allows for a **tractable and consistent** treatment of nuclear matter, atomic nuclei and neutron-star crusts.

The energy of a lump of matter is expressed as ($q = n, p$)

$$E = \int \mathcal{E} \left[\rho_q(\mathbf{r}), \nabla \rho_q(\mathbf{r}), \tau_q(\mathbf{r}), \mathbf{J}_q(\mathbf{r}), \tilde{\rho}_q(\mathbf{r}) \right] d^3\mathbf{r}$$

where $\rho_q(\mathbf{r}), \tau_q(\mathbf{r}) \dots$ are functionals of $\varphi_{1k}^{(q)}(\mathbf{r})$ and $\varphi_{2k}^{(q)}(\mathbf{r})$

$$\begin{pmatrix} h_q(\mathbf{r}) - \lambda_q & \Delta_q(\mathbf{r}) \\ \Delta_q(\mathbf{r}) & -h_q(\mathbf{r}) + \lambda_q \end{pmatrix} \begin{pmatrix} \varphi_{1k}^{(q)}(\mathbf{r}) \\ \varphi_{2k}^{(q)}(\mathbf{r}) \end{pmatrix} = E_k^{(q)} \begin{pmatrix} \varphi_{1k}^{(q)}(\mathbf{r}) \\ \varphi_{2k}^{(q)}(\mathbf{r}) \end{pmatrix}$$

$$h_q \equiv -\nabla \cdot \frac{\delta E}{\delta \tau_q} \nabla + \frac{\delta E}{\delta \rho_q} - i \frac{\delta E}{\delta \mathbf{J}_q} \cdot \nabla \times \boldsymbol{\sigma}, \quad \Delta_q \equiv \frac{\delta E}{\delta \tilde{\rho}_q}$$

Effective nuclear energy density functional

- In principle, one can construct the nuclear functional from realistic nucleon-nucleon forces (i.e. fitted to experimental nucleon-nucleon phase shifts) using many-body methods

$$\mathcal{E} = \frac{\hbar^2}{2M}(\tau_n + \tau_p) + A(\rho_n, \rho_p) + B(\rho_n, \rho_p)\tau_n + B(\rho_p, \rho_n)\tau_p \\ + C(\rho_n, \rho_p)(\nabla\rho_n)^2 + C(\rho_p, \rho_n)(\nabla\rho_p)^2 + D(\rho_n, \rho_p)(\nabla\rho_n) \cdot (\nabla\rho_p) \\ + \text{Coulomb, spin-orbit and pairing}$$

Drut et al., Prog.Part.Nucl.Phys.64(2010)120.

- But difficult task so in practice, we use phenomenological (Skyrme) functionals

Bender et al., Rev.Mod.Phys.75, 121 (2003).

Phenomenological corrections for atomic nuclei

For atomic nuclei, we add the following corrections not taken into account in Skyrme functionals:

$$E_{\text{corr}} = E_W + E_{\text{coll}}$$

- Wigner energy

$$E_W = V_W \exp \left\{ -\lambda \left(\frac{N-Z}{A} \right)^2 \right\} + V'_W |N-Z| \exp \left\{ -\left(\frac{A}{A_0} \right)^2 \right\}$$

- rotational and vibrational spurious collective energy

$$E_{\text{coll}} = E_{\text{rot}}^{\text{crank}} \left\{ b \tanh(c|\beta_2|) + d|\beta_2| \exp\{-l(|\beta_2| - \beta_2^0)^2\} \right\}$$

Construction of the functional

Experimental data:

- 2149 measured nuclear masses with $Z, N \geq 8$
- compressibility $230 \leq K_v \leq 250$ MeV
- charge radius of ^{208}Pb , $R_c = 5.501 \pm 0.001$ fm
- symmetry energy $J = 30$ MeV
- isoscalar effective mass $M_s^*/M = 0.8$

N-body calculations with realistic forces:

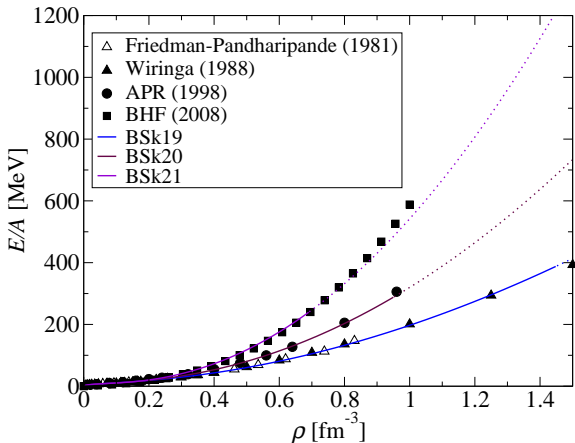
- equation of state of pure neutron matter
- 1S_0 pairing gaps in symmetric and neutron matter
- Landau parameters, stability against spin and spin-isospin phase transitions

Goriely, Chamel, Pearson, Phys.Rev.C82,035804 (2010).

With these constraints, the functional is expected to be well suited for describing the interior of neutron stars.

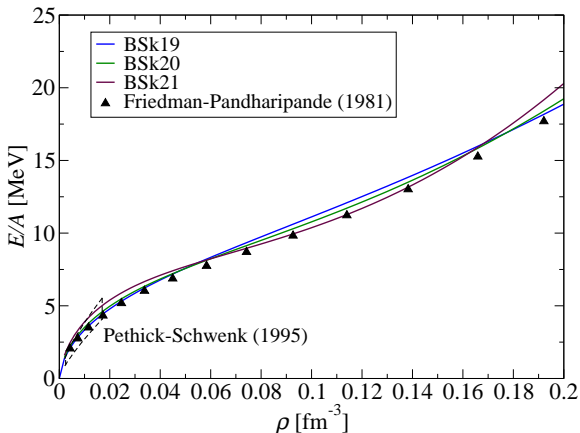
Neutron-matter equation of state at high densities

We have constructed a family of three different Skyrme functionals BSk19, BSk20 and BSk21 spanning the range of realistic neutron-matter equations of state.



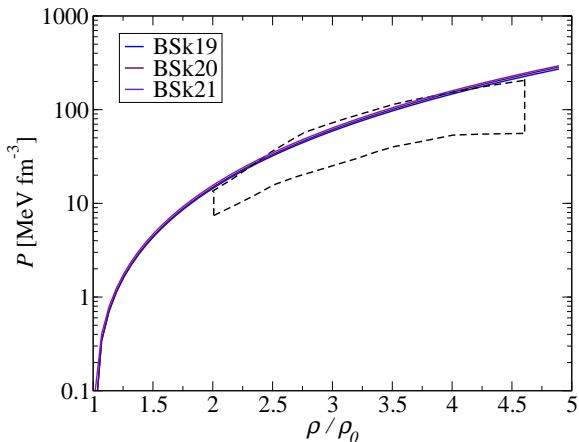
Neutron-matter equation of state at low densities

All three functionals yield similar neutron-matter equations of state at subsaturation densities consistent with microscopic calculations using realistic nucleon-nucleon interactions



Constraints from heavy-ion collisions

Our functionals are consistent with the pressure of symmetric nuclear matter inferred from Au+Au collisions



Danielewicz et al., Science 298, 1592 (2002).

Pairing energy density functional

The pairing functional is generally parametrized as

$$\mathcal{E}_{\text{pair}} = \frac{1}{4} \sum_{q=n,p} v^{\pi q}[\rho_n, \rho_p] \tilde{\rho}_q^2, \quad v^{\pi q}[\rho_n, \rho_p] = v_{\pi q}^{\Lambda} \left(1 - \eta \left(\frac{\rho}{\rho_0} \right)^{\alpha} \right)$$

- not enough flexibility to fit pairing gaps in infinite nuclear matter and in nuclei (\Rightarrow isospin dependence)
- not suitable for a global fit to atomic masses.

Instead, $v^{\pi q}[\rho_n, \rho_p]$ is constructed so as to reproduce *exactly* a given 1S_0 pairing gap function $\Delta_q(\rho_n, \rho_p)$ in nuclear matter
Chamel, Goriely, Pearson, Nucl.Phys.A812,72 (2008).
Goriely, Chamel, Pearson, PRL 102, 152503 (2009).

This procedure provides a one-to-one correspondence between pairing in nuclei and pairing in infinite nuclear matter.

Analytical expression of the pairing strength

The pairing strength can be expressed in analytical form

$$v^{\pi q}[\rho_n, \rho_p] = -\frac{8\pi^2}{I_q(\rho_n, \rho_p)} \left(\frac{\hbar^2}{2M_q^*(\rho_n, \rho_p)} \right)^{3/2}$$

$$I_q(\rho_n, \rho_p) = \sqrt{\varepsilon_F^{(q)}} \left[2 \log \left(\frac{2\varepsilon_F^{(q)}}{\Delta_q} \right) + \Lambda \left(\frac{\varepsilon_\Lambda}{\varepsilon_F^{(q)}} \right) \right]$$

$$\Lambda(x) = \log(16x) + 2\sqrt{1+x} - 2 \log \left(1 + \sqrt{1+x} \right) - 4$$

NB: s.p. energy cutoff ε_Λ above the Fermi level $\varepsilon_F^{(q)}$.

Chamel, Phys. Rev. C 82, 014313 (2010)

- exact fit of the given gap function $\Delta_q(\rho_n, \rho_p)$
- automatic renormalization of the pairing strength with ε_Λ
- no free parameters apart from ε_Λ

Pairing cutoff and experimental phase shifts

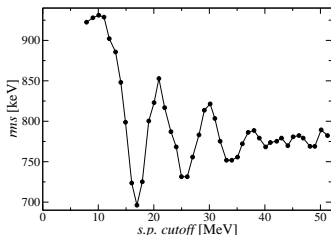
In the limit of vanishing density, the pairing strength

$$v^\pi[\rho_q \rightarrow 0] = -\frac{4\pi^2}{\sqrt{\varepsilon_\Lambda}} \left(\frac{\hbar^2}{2M_q} \right)^{3/2}$$

should coincide with the bare force in the 1S_0 channel.

A fit to the experimental 1S_0 NN phase shifts yields $\varepsilon_\Lambda \sim 7 - 8$ MeV.

Esbensen et al., Phys. Rev. C 56, 3054 (1997).



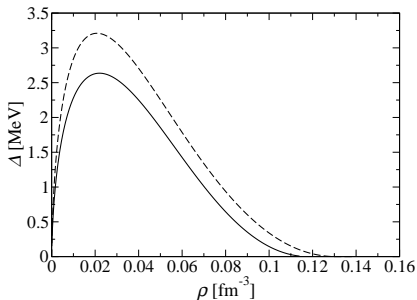
On the other hand, a better mass fit can be obtained with $\varepsilon_\Lambda \sim 16$ MeV while convergence is achieved for $\varepsilon_\Lambda \gtrsim 40$ MeV.

Goriely et al., Nucl.Phys.A773(2006),279.

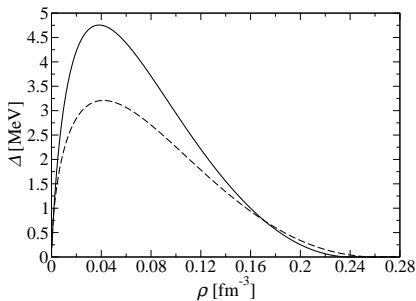
Choice of microscopic pairing gaps

1S_0 pairing gaps obtained from **Brueckner calculations taking into account medium polarization effects**. For comparison, we also constructed a functional (BSk16) by fitting BCS pairing gaps (dashed lines).

Neutron matter



Symmetric nuclear matter



Cao et al., Phys.Rev.C74,064301(2006).

Neutron vs proton pairing

- Because of possible **charge symmetry breaking effects**, proton and neutron pairing strengths may not be equal

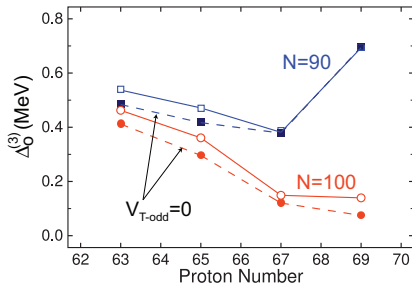
$$v^{\pi n}[\rho_n, \rho_p] \neq v^{\pi p}[\rho_n, \rho_p]$$

- The neglect of **polarization effects in odd nuclei** (equal filling approximation) is corrected by “staggered” pairing
⇒ renormalization factors f_q^{\pm} ($f_n^+ \equiv 1$ by definition)

From the global fit

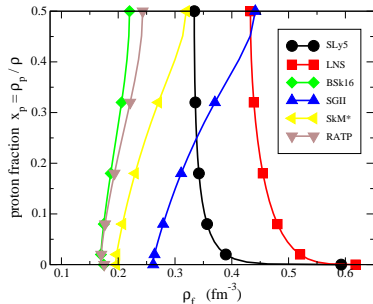
$$f_n^- / f_n^+ \simeq f_p^- / f_p^+ \text{ and } f_n^- > f_n^+.$$

This is in agreement with a recent analysis by Bertsch et al. *Phys.Rev.C79(2009),034306*

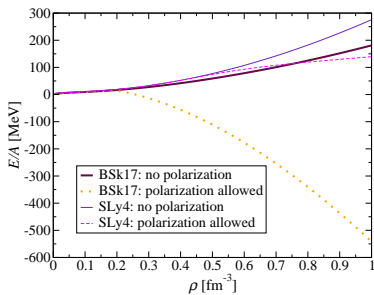


Ferromagnetic instability

Unlike microscopic calculations, conventional Skyrme functionals predict a ferromagnetic transition in nuclear matter sometimes leading to a ferromagnetic collapse of neutron stars.



Margueron et al.,
J.Phys.G36(2009),125102.



Chamel et al.,
Phys.Rev.C80(2009),065804.

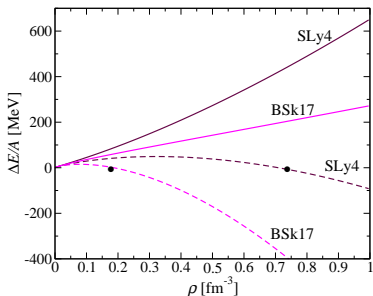
Spin and spin-isospin instabilities

Skyrme functional in polarized homogeneous nuclear matter

$$\mathcal{E}_{\text{Sky}}^{\text{pol}} = \mathcal{E}_{\text{Sky}}^{\text{unpol}} + C_0^s \mathbf{s}^2 + C_1^s (\mathbf{s}_n - \mathbf{s}_p)^2 + C_0^T \mathbf{s} \cdot \mathbf{T} + C_1^T (\mathbf{s}_n - \mathbf{s}_p) \cdot (\mathbf{T}_n - \mathbf{T}_p)$$

with $\mathbf{s}_q = \rho_{q\uparrow} - \rho_{q\downarrow}$ and $\mathbf{T}_q = \tau_{q\uparrow} - \tau_{q\downarrow}$.

Spurious spin and spin-isospin instabilities arise from the C_0^T and C_1^T terms ($\Rightarrow J^2$ terms) in the Skyrme functional.



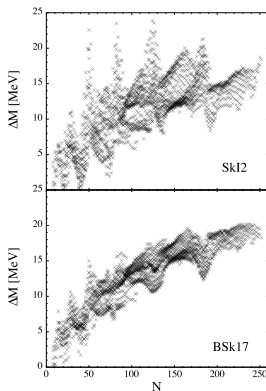
Difference between the energy per particle in fully polarized neutron matter and in unpolarized neutron matter with (dashed line) and without (solid line) the J^2 terms.

Chamel&Goriely, Phys.Rev.C82, 045804 (2010)

Impact of the J^2 terms

Dropping the J^2 terms and their associated time-odd parts

- removes spin and spin-isospin instabilities at any $T \geq 0$
- prevents an anomalous behavior of the entropy
- improves the values of Landau parameters (especially G'_0) and the sum rules.



Adding or removing a posteriori the J^2 terms without refitting the functional can induce large errors!

Chamel & Goriely, Phys.Rev.C82, 045804 (2010)

More about the J^2 terms

On the other hand dropping the J^2 terms leads to

- unrealistic effective masses in polarized matter

$$\frac{\hbar^2}{2M_{q\sigma}^*} = \frac{\hbar^2}{2M_q^*} \pm \left[s(C_0^T - C_1^T) + 2s_q C_1^T \right] \Rightarrow M_{q\uparrow}^* = M_{q\downarrow}^* = M_q^*$$

- self-interaction errors (non-vanishing of the potential energy in the one-particle limit).

Chamel, Phys. Rev. C 82, 061307(R) (2010).

Instabilities can be removed *with* the J^2 terms by adding density-dependent terms in C_0^T and C_1^T . But only for $T = 0$.

Chamel, Goriely, Pearson, Phys.Rev.C80(2009),065804.

HFB mass tables

Results of the fit on the 2149 measured masses with $Z, N \geq 8$

	HFB-19	HFB-20	HFB-21	FRDM
$\sigma(M)$ [MeV]	0.583	0.583	0.577	0.656
$\bar{\epsilon}(M)$ [MeV]	-0.038	0.021	-0.054	0.058
$\sigma(M_{nr})$ [MeV]	0.803	0.790	0.762	0.910
$\bar{\epsilon}(M_{nr})$ [MeV]	0.243	0.217	-0.086	0.047
$\sigma(S_n)$ [MeV]	0.502	0.525	0.532	0.399
$\bar{\epsilon}(S_n)$ [MeV]	-0.015	-0.012	-0.009	-0.001
$\sigma(Q_\beta)$ [MeV]	0.612	0.620	0.620	0.498
$\bar{\epsilon}(Q_\beta)$ [MeV]	0.027	0.024	0.000	0.004
$\sigma(R_C)$ [fm]	0.0283	0.0274	0.0270	0.0545
$\bar{\epsilon}(R_C)$ [fm]	-0.0032	0.0009	-0.0014	-0.0366
$\theta(^{208}\text{Pb})$ [fm]	0.140	0.140	0.137	

Goriely, Chamel, Pearson, *Phys.Rev.C82,035804* (2010).

Nuclear-matter properties

	BSk19	BSk20	BSk21
a_v [MeV]	-16.078	-16.080	-16.053
ρ_0 [fm ⁻³]	0.1596	0.1596	0.1582
J [MeV]	30.0	30.0	30.0
K_v [MeV]	237.3	241.4	245.8
K' [MeV]	297.8	282.2	274.1
L [MeV]	31.9	37.4	46.6
K_{sym} [MeV]	-191.4	-136.5	-37.2
K_{τ} [MeV]	-342.8	-317.1	-264.6
K_{coul} [MeV]	-5.093	-5.158	-5.186
M_s^*/M	0.80	0.80	0.80
M_v^*/M	0.61	0.65	0.71

Goriely, Chamel, Pearson, Phys.Rev.C82,035804 (2010).

Description of neutron star crust below neutron drip

The equilibrium structure of the outer crust is determined using the BPS model with experimental masses when available and HFB mass tables otherwise.

BPS model: cold catalyzed matter at $T = 0$

Minimize the energy per nucleon ε/n of a body centered cubic crystal with a single nuclear species (A,Z) at lattice sites

$$\varepsilon = n_N M\{A, Z\} + \varepsilon_e + \varepsilon_L$$

Baym, Pethick, Sutherland (BPS), Astr. J.170(1971)299.

Equilibrium nucleus in the densest layer before neutron drip

	Z	N	A	n_{min} (fm^{-3})	n_{max} (fm^{-3})
HFB-19	38	88	126	2.46×10^{-4}	2.63×10^{-4}
HFB-20	38	88	126	2.60×10^{-4}	2.63×10^{-4}
HFB-21	38	86	124	2.45×10^{-4}	2.57×10^{-4}

Pearson, Goriely and Chamel, Phys.Rev.C in press.

Description of neutron star crust beyond neutron drip

The equilibrium structure of the inner crust is determined with the Extended Thomas-Fermi (up to 4th order)+Strutinsky Integral method (ETFSI).

- Pairing is expected to have a small impact on the composition and is therefore neglected.
- Nuclei are assumed to be spherical.

Onsi et al., Phys.Rev.C77,065805 (2008).

Advantages of ETFSI method

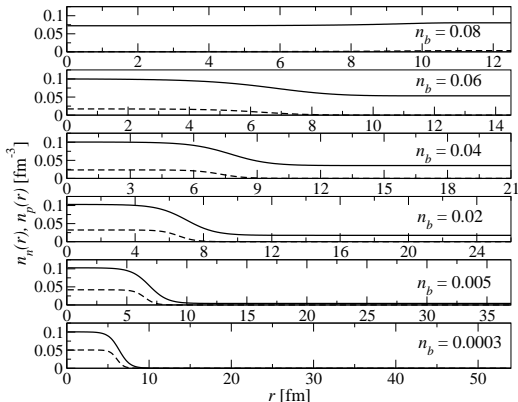
- very fast approximation to the full Hartree-Fock method
- avoids the difficulties related to boundary conditions but include proton shell effects (neutron shell effects are generally much smaller and can be omitted)

Chamel et al., Phys.Rev.C75(2007),055806.

Ground-state composition of the inner crust

Results for BSk14

n_b (fm $^{-3}$)	Z	A
0.0003	50	200
0.001	50	460
0.005	50	1140
0.01	40	1215
0.02	40	1485
0.03	40	1590
0.04	40	1610
0.05	20	800
0.06	20	780



Onsi, Dutta, Chatri, Goriely, Chamel and Pearson, Phys.Rev.C77,065805 (2008).

With BSk19, BSk20 and BSk21, only $Z = 40$ is found.

Neutron superfluidity in neutron-star crusts

Most microscopic calculations of neutron superfluidity have been performed in uniform matter. How does the crust affect neutron superfluidity?

In the BCS approximation

$$\Delta_{\alpha\mathbf{k}} = -\frac{1}{2} \sum_{\beta} \sum_{\mathbf{k}'} \bar{v}_{\alpha\mathbf{k}\alpha-\mathbf{k}\beta\mathbf{k}'\beta-\mathbf{k}'}^{\text{pair}} \frac{\Delta_{\beta\mathbf{k}'}}{E_{\beta\mathbf{k}'}} \tanh \frac{E_{\beta\mathbf{k}'}}{2T}$$

$$\bar{v}_{\alpha\mathbf{k}\alpha-\mathbf{k}\beta\mathbf{k}'\beta-\mathbf{k}'}^{\text{pair}} = \int d^3r v^{\pi}[\rho_n(\mathbf{r}), \rho_p(\mathbf{r})] |\varphi_{\alpha\mathbf{k}}(\mathbf{r})|^2 |\varphi_{\beta\mathbf{k}'}(\mathbf{r})|^2$$

$$E_{\alpha\mathbf{k}} = \sqrt{(\varepsilon_{\alpha\mathbf{k}} - \mu)^2 + \Delta_{\alpha\mathbf{k}}^2}$$

$\varepsilon_{\alpha\mathbf{k}}$, μ and $\varphi_{\alpha\mathbf{k}}(\mathbf{r})$ are obtained from band structure calculations

Chamel et al., Phys.Rev.C81,045804 (2010).

Neutron pairing gaps

n_n^f is the density of unbound neutrons

Δ_F is the average gap around the Fermi level

Δ_u is the gap in neutron matter at density n_n^f

$\bar{\Delta}_u$ is the gap in neutron matter at density n_n

n_b [fm^{-3}]	n_n^f [fm^{-3}]	Δ_F [MeV]	Δ_u [MeV]	$\bar{\Delta}_u$ [MeV]
0.07	0.060	1.44	1.79	1.43
0.065	0.056	1.65	1.99	1.65
0.06	0.051	1.86	2.20	1.87
0.055	0.047	2.08	2.40	2.10
0.05	0.043	2.29	2.59	2.33

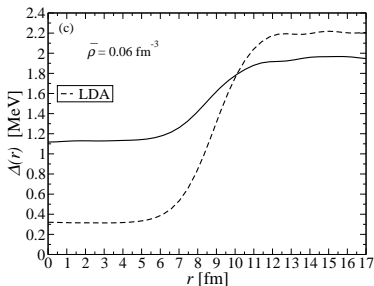
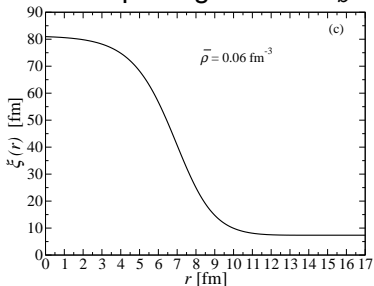
- the nuclear clusters lower the gap by 10 – 20%
- both bound and unbound neutrons contribute to the gap
- the critical temperature is given by $T_c \simeq 0.567\Delta_F$

Pairing field and local density approximation

The effects of inhomogeneities on neutron superfluidity can be directly seen in the pairing field

$$\Delta_n(\mathbf{r}) = -\frac{1}{2} v^{\pi n} [\rho_n(\mathbf{r}), \rho_p(\mathbf{r})] \tilde{\rho}_n(\mathbf{r}), \quad \tilde{\rho}_n(\mathbf{r}) = \sum_{\alpha, \mathbf{k}}^{\Lambda} |\varphi_{\alpha \mathbf{k}}(\mathbf{r})|^2 \frac{\Delta_{\alpha \mathbf{k}}}{E_{\alpha \mathbf{k}}}$$

Neutron pairing field for $n_b = 0.06 \text{ fm}^{-3}$ at $T = 0$



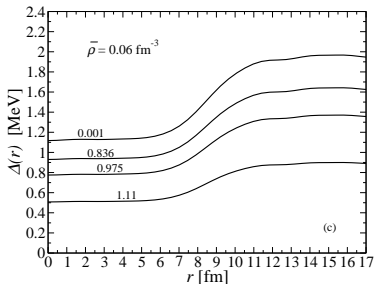
Pairing field at finite temperature

At $T > 0$, the neutron pairing field is given by

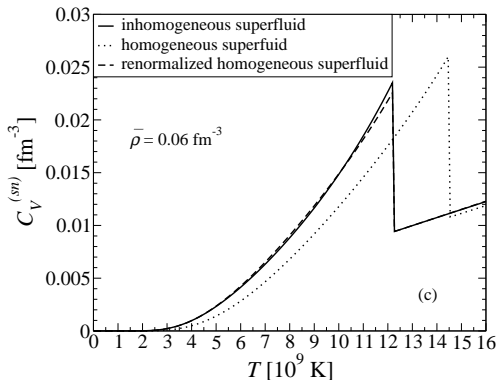
$$\Delta_n(\mathbf{r}) = -\frac{1}{2} v^{\pi n} [\rho_n(\mathbf{r}), \rho_p(\mathbf{r})] \tilde{\rho}_n(\mathbf{r}), \quad \tilde{\rho}_n(\mathbf{r}) = \sum_{\alpha, \mathbf{k}}^{\Lambda} |\varphi_{\alpha \mathbf{k}}(\mathbf{r})|^2 \frac{\Delta_{\alpha \mathbf{k}}}{E_{\alpha \mathbf{k}}} \tanh \frac{E_{\alpha \mathbf{k}}}{2T}$$

Neutron pairing field for $n_b = 0.06 \text{ fm}^{-3}$

The superfluid becomes more and more homogeneous as T approaches T_c



Impact on thermodynamic quantities : specific heat



- Band structure effects are small. This remains true for non-superfluid neutrons.

Chamel et al, Phys. Rev. C 79, 012801(R) (2009)

- The renormalization of T_c comes from the density dependence of the pairing strength.

How “free” are neutrons in neutron-star crusts?

The crust has a strong impact on the neutron superfluid hydrodynamics.

Pethick, Chamel, Reddy, Prog.Theor.Phys.Sup.186(2010)9.

n_b (fm ⁻³)	n_n^f/n_n (%)	n_n^c/n_n^f (%)
0.0003	20.0	82.6
0.001	68.6	27.3
0.005	86.4	17.5
0.01	88.9	15.5
0.02	90.3	7.37
0.03	91.4	7.33
0.04	88.8	10.6
0.05	91.4	30.0
0.06	91.5	45.9
0.08	104	64.8

The density n_n^c of “conduction” neutrons (i.e. superfluid neutron density) can be much smaller than the density n_n^f of unbound neutrons!

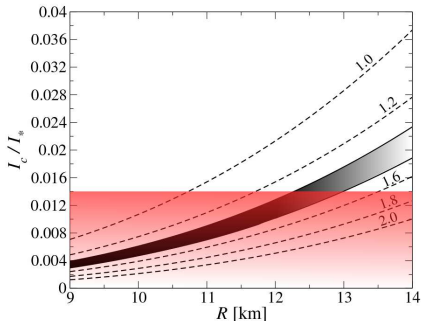
Do we understand pulsar glitches?

Large pulsar glitches are generally interpreted as sudden angular momentum transfers between the “free” (=conducting!) neutrons in the crust and the rest of the star.

$$\frac{I_c}{I} \geq \frac{\Omega}{|\dot{\Omega}_{\text{av}}|} \frac{1}{\tau} \sum_i \frac{\Delta\Omega_i}{\Omega} \quad (\text{red})$$

Constraints from X-ray bursters
and LMXB (grey)

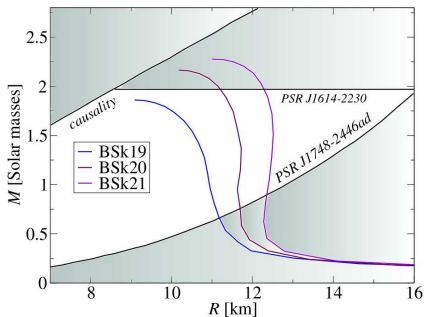
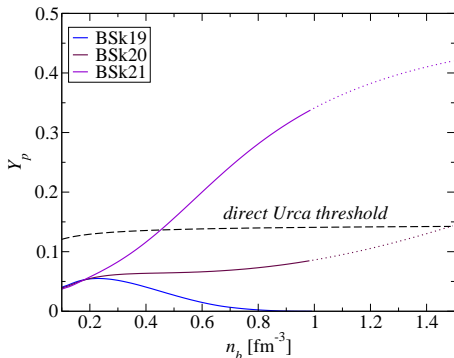
Steiner et al., ApJ722(2010), 33.



- Glitching pulsars have a very low mass
- Neutron-star core is involved in glitches
- Nuclear pastas?

Unified equation of state of neutron stars

All regions of neutron stars can be described using the same functional (n , p , e , μ matter in the core).



	n_{caus} (fm^{-3})	$\mathcal{M}_{\text{max}}/\mathcal{M}_{\odot}$	R (km)	n_{max} (fm^{-3})
BSk19	1.45	1.86 (1.84)	9.13	1.45
BSk20	0.98	2.14 (2.20)	10.6	0.98
BSk21	0.99	2.28 (2.3)	11.0	0.97

Summary

Take home message

The nuclear energy density functional (EDF) theory allows for a unified treatment of all regions of neutron stars.

- 1 We have developed a family of Skyrme EDF constrained by experiments and N-body calculations:
 - they give an excellent fit to essentially all nuclear mass data ($\sigma \lesssim 0.6$ MeV)
 - they reproduce various properties of infinite nuclear matter (EoS, pairing gaps, *etc*)
- 2 These functionals can be further constrained by neutron-star observations